

CALCULATION OF THE ELECTRIC FIELD AT THE EDGE OF THE OPERATION REGION OF THE CATHODE STRIP CHAMBERS OF CMS ME1/1 STATION

A. Yu. Kamenev, P. V. Moissenz

Joint Institute for Nuclear Research, Dubna

Distortion of the electric field near the edge of the operation region of Cathode Strip Chamber (CSC) of the first Muon Endcap Station (ME1/1) of the Compact Muon Solenoid (CMS) is studied. The distortions of the shape and the magnitude of the electric field that arise from the presence of the insulating frame, which supports the anode wire array, are investigated. The electric field calculation is done with the aid of the Boundary Elements Method.

В работе исследованы искажения электрического поля вблизи края рабочей области катодно-стриповой камеры первой мюонной станции торцевой части детектора CMS (Compact Muon Solenoid). Рассмотрены искажения формы и величины электрического поля, вносимые присутствием изолирующей рамки, на которую крепится массив анодных проволок. Расчет электрического поля выполнен с помощью метода граничных элементов.

PACS: 29.40.Cs, 29.40.Gx

INTRODUCTION

Standalone alignment of the Cathode Strip Chambers (CSC) [1] in the Muon Endcap Station 1 (ME1/1) of CMS detector relies on the fact that the edge regions of the adjacent CSCs overlap. The overlapping region consists of first 5 cathode strips from the edge of CSC. Thus, one should investigate performance of the CSC in the edge region. The electric field distribution at the edge of the CSC could be distorted due to the presence of dielectric supporting frame and because the anode wires in ME1/1 chambers are not normal to that frame. We should be aware that the electric field near the 2nd strip is equal to the field in the central region of the CSC as the φ coordinate of the track hit is reconstructed from the ratio of the signals from 3 adjacent strips [2]. The desired precision of φ coordinate measurement for single CSC layer is $120\ \mu\text{m}$ and the edge effects should not distort this resolution. For this task the Boundary Elements Method [3] was applied.

1. IMPLEMENTATION OF BOUNDARY ELEMENTS METHOD

As for general physics, the problem is stated as follows: there is a set of conductors and dielectrics and we know the potential at each conductor and electric permittivity of each dielectric. We should calculate the electric field produced by this system.

At each point of the surfaces the electric field should satisfy the boundary conditions: the potential at the conductors surfaces should be equal to the predefined values and the normal component of \mathbf{D} vector should be continuous at the dielectric surfaces. If we find the distribution of electric charges that would satisfy the boundary conditions we will be able to calculate the electric field at any point.

Let us divide the surfaces of the conductors and dielectrics into small (relative to the size of the system) elements. Within (or, near) each element we define a point (2 points for dielectric surface), which will be used to check the boundary condition at that element. Hence, we obtain a system of equations of the following type:

$$\varphi_i = \varphi_0, \quad \varepsilon_2 E_j^{n2} - \varepsilon_1 E_j^{n1} = 0, \quad (1)$$

here i, j are the indices of elements; φ_0 — given potential; $\varepsilon_1, \varepsilon_2$ — electric permittivity of dielectrics that consist in the interface at the element j ; $E_j^{n1,2}$ — component of electric field intensity normal to the surface of the element j . Figure 1 shows the implementation of workpoints at which the boundary conditions are true. The center of element local reference frame is at point 0. For the surface between dielectric both workpoints are needed, but

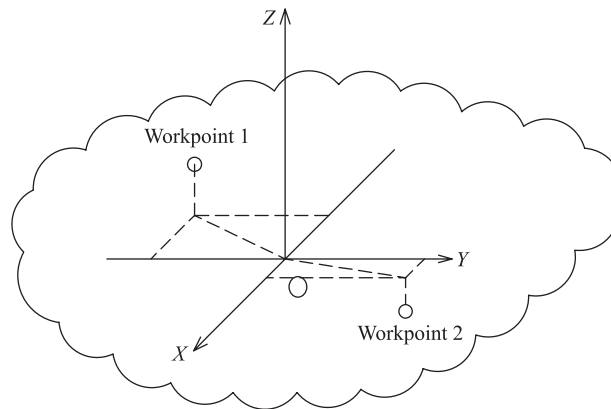


Fig. 1. Workpoints and surface element

for conductor surface only one point is needed which could even be within the surface (for example, for flat rectangular element). The placement of workpoints depends on the calculation algorithm of field from the surface element. In general, the closer workpoints are to the surface is the better, but if the element is represented as a discrete set of equally charged points within the surface the field very close to the surface could be calculated wrong. Knowing how to calculate the electric field from the element at any point in local reference frame and having the transition rules to convert the result into general reference frame one can obtain the resulting electric field.

Knowing the distribution of charges on surfaces, one can calculate the electric potential and field intensity at any point X by following sums:

$$\varphi(X) = \sum_{i=1}^N a_i(X)q_i, \quad \mathbf{E}(X) = \sum_{i=1}^N \mathbf{b}_i(X)q_i. \quad (2)$$

Here N — total number of elements; a_i and \mathbf{b}_i — coefficients that depend on the shape of the element i and its relative position to the point X . Substitution of equations (2) into system (1) gives:

$$\sum_{i=1}^N a_i^k q_i = \varphi^k, \tag{3}$$

$$\sum_{i=1}^N [\varepsilon_2(\mathbf{b}_i^{m2} \mathbf{n}^2) - \varepsilon_1(\mathbf{b}_i^{m1} \mathbf{n}^1)] q_i = 0.$$

Here $\mathbf{n}^{1,2}$ — unitary vector normal to the surface; k — index for conductor elements; m — index for dielectric elements.

This is the system of N linear equations with N unknown q_i . It could be solved by any convenient method.

2. CHECKING OF THE APPROACH

This approach is conveniently realizable within object oriented programming style. One should create as many classes as the number of types of elements. The main task (the edge of CSC) could be divided into rectangular flat elements and linear elements (anode wires). Below, the implementation of rectangular elements is checked.

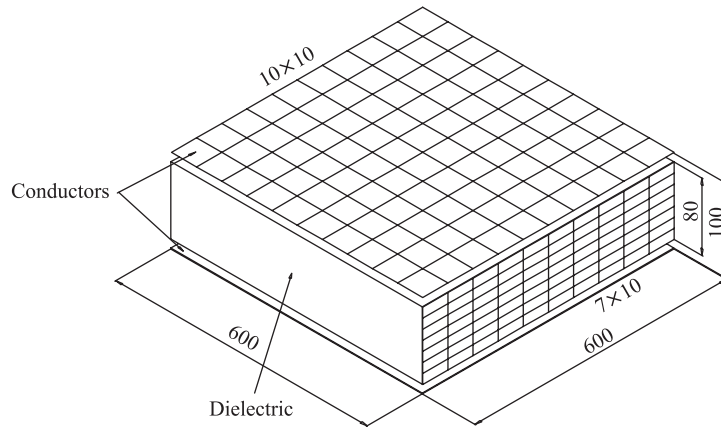


Fig. 2. Capacitor and its elements (distances — in μm)

The realization of rectangular elements was checked on the flat capacitor problem. Figure 2 shows the configuration of conductors and dielectrics for this case. All dimensions are in μm .

Both conductors were divided by 10×10 square elements with size 0.06 mm (the dimensions are mostly for reference and could be scaled). Corresponding surfaces of dielectric were divided into the same elements. Lateral sides of dielectric were divided into 7×10 rectangular elements. The gap between conductors was 0.1 mm and the height of dielectric

was 0.08 mm. The bottom conductor plate has 1000 V potential and the top plate was under 1000 V potential. Two cases were investigated: $\epsilon = 1$ and $\epsilon = 5$. Figure 3 shows field lines in capacitor for different electric permittivities. One can see that the field near the center is uniform, and outer field lines in the case of higher permittivity are retracted inside dielectric.

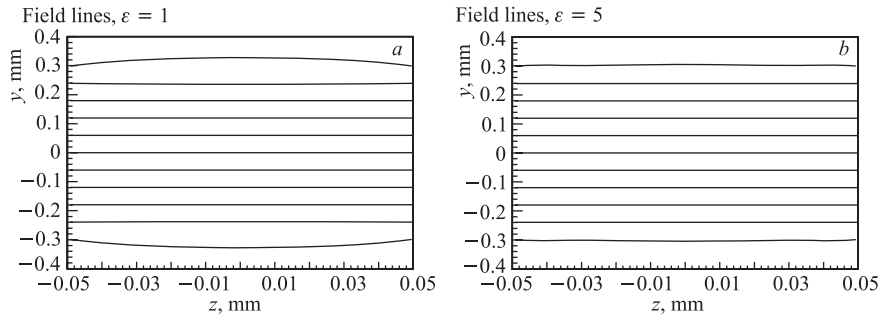


Fig. 3. Field lines in capacitor for different electric permittivities

The electric field intensity along field lines is shown in Fig. 4. The solid line corresponds to the central field line from Fig. 3 and the dotted line corresponds to the outer line. One

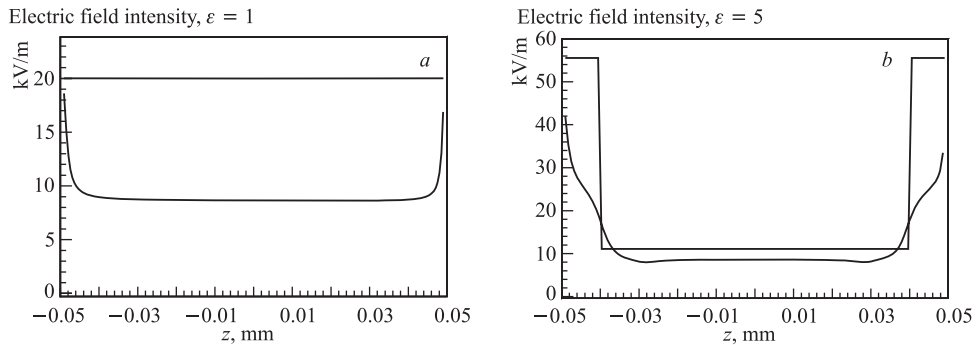


Fig. 4. Electric field intensity along field lines

can see that for the case $\epsilon = 1$ the electric field intensity is uniform along line and is equal $2000 \text{ V}/0.1 \text{ mm} = 20 \text{ kV/m}$. For the case $\epsilon = 5$ there is a leap in field intensity on the boundary of dielectric and the field intensity within dielectric is exactly 5 times less than outside of it. If we integrate the electric field intensity along central line for the case $\epsilon = 5$ we obtain the 2000 V difference between plates. As one can see, the calculations are in good agreement with theoretical considerations, so the implementation of rectangular elements is considered to be right. The actual formulas for the electric field of the rectangular surface element are given in Appendix A. These formulas are obtained with the calculation code «Mathematica» from Wolfram Research [4].

Check of the implementation of linear element (wires in the CSC edge problem) was made within calculation of the edge of CSC problem. The actual formulas for the electric field of the linear element are given in Appendix B.

3. DESCRIPTION OF THE EDGE OF ME1/1 CATHODE STRIP CHAMBER

The edge of ME1/1 CSC layer is shown on Fig. 5. Anode plane consists of wires with diameter 0.03 mm and spacing 2.5 mm. Anode-cathode distance is 3.5 mm. There are two insulating dielectric frames. The bottom frame (in Fig. 5) is used to support the anode wires

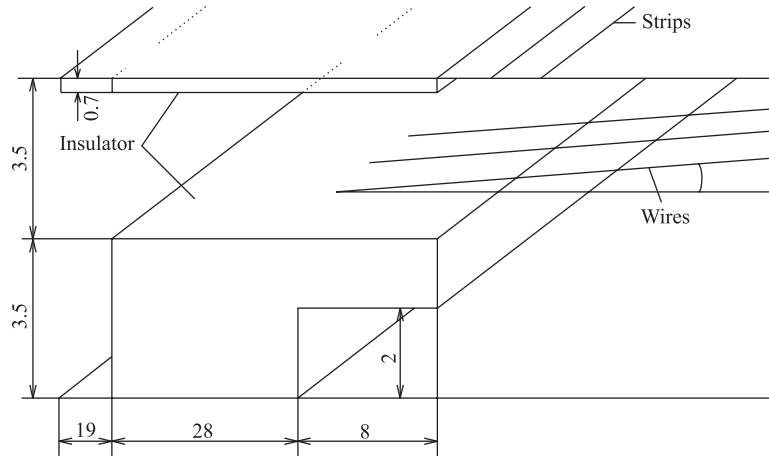


Fig. 5. Layout of the CSC layer edge (all distances — in mm)

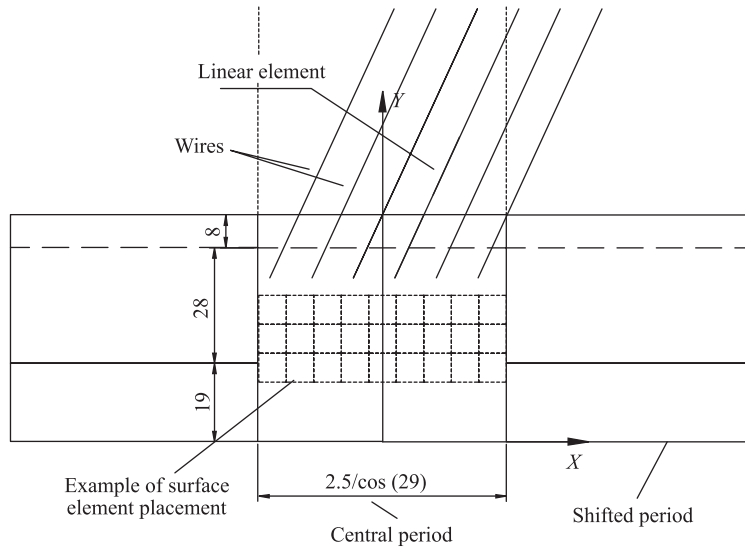


Fig. 6. Placement of the surface elements

and the high voltage distribution system. The top frame provides isolation of high voltage soldering on the bottom frame from the top cathode. Both frames are made from dielectric

with $\varepsilon = 5.4$. Top cathode is cut into strips. The outer edge of the first strip is at the end of top insulator frame (see Fig. 5). Wires in CSC are inclined at the angle 29° to the central strip cut.

We use the signals from 3 adjacent strips to reconstruct the φ coordinate of muon track. So, we should check if the electron drift and electron avalanche within the second strip are affected by the distortions of electric field. As the CSC has the trapezoidal shape, strips has the width $\sim 4\text{--}7$ mm in the different regions of CSC. So, if we find out that electric field at the distance of 4 mm from insulator frames is actually the same as in the middle of CSC, we could assume that the performance of CSC in the edge region is the same as in the center of it.

Placement of surface elements is shown in Fig. 6. As the structure is periodical in the direction parallel to the supporting frame, the elements are distributed only within one spatial period. All the charges in the other periods are supposed to be equal to them. During the calculations one should add the influence of elements that are identical to the central ones, but shifted to the left or to the right by certain number of periods. In this work, ± 40 periods were considered. Increase in this number doesn't change the results but increased the time of calculation.

4. RESULTS OF CALCULATIONS

First of all, the electric field far from edge of CSC was calculated. Then, it was compared with theoretical formulas for the case of infinite number of wires of infinite length between two cathodes. The results are shown in Fig. 7. It is seen that Z -coordinate is along anode-cathode

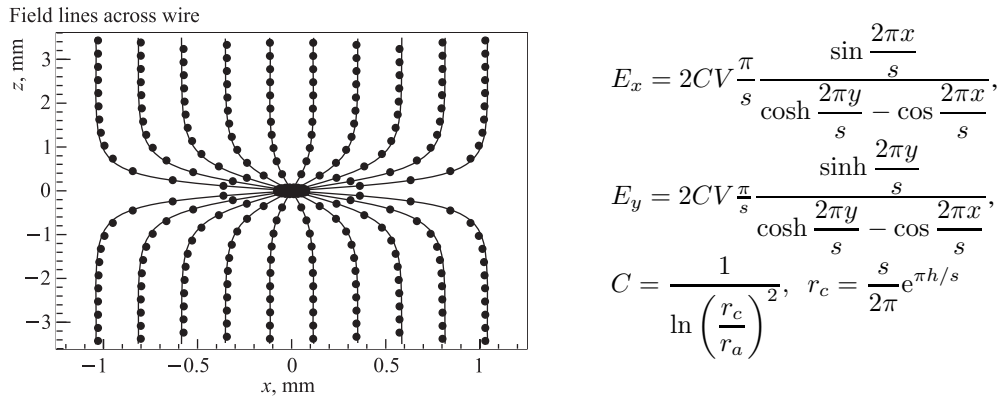


Fig. 7. Field in the middle of CSC: solid lines — our results; dots — theoretical considerations

direction and x -coordinate is between anode wires. Solid lines are the current result and the points represent the theoretical calculations by formulas on the right [5]. There is a good agreement here and one can conclude that the implementation of the linear elements for the wires is correct.

Field lines originating from the points on the wire nearest to cathodes are shown in Fig. 8. Edges of the insulator frames are shown on the left. Abscissa zero is at the end of frames.

Horizontal line is a wire. Cathodes are at the top and bottom of the picture. Figure 9 shows the deviation of the field lines from Fig. 8 from their origin points. Solid line is for bottom field lines and the dashed one is for the top. One can see that at the distance 4 mm from the frame edge the drifting primary electron could be shifted across strips for not more than $50 \mu\text{m}$. This will not significantly affect desired $120 \mu\text{m}$ precision.

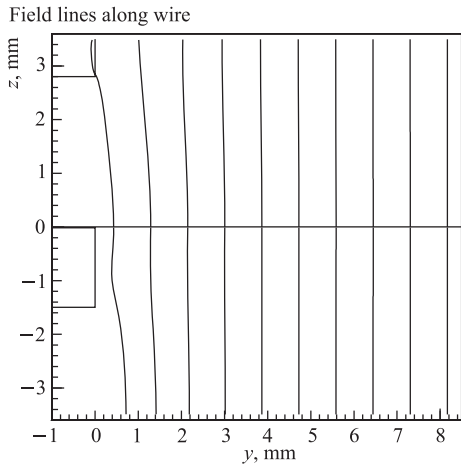


Fig. 8. Field lines along wire

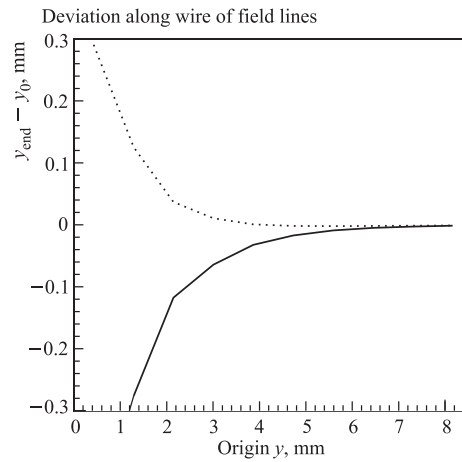


Fig. 9. Deviation of field lines from their origin

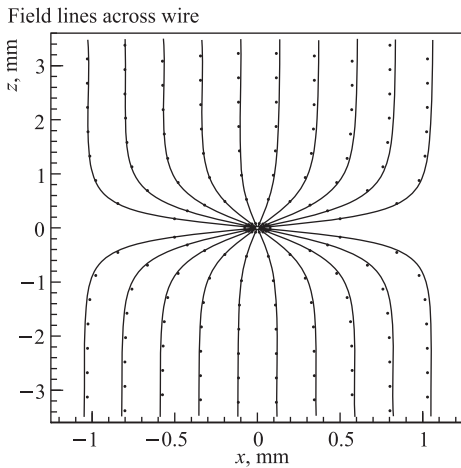


Fig. 10. Field lines across wire near the edge. Solid lines — our results; dots — theoretical considerations

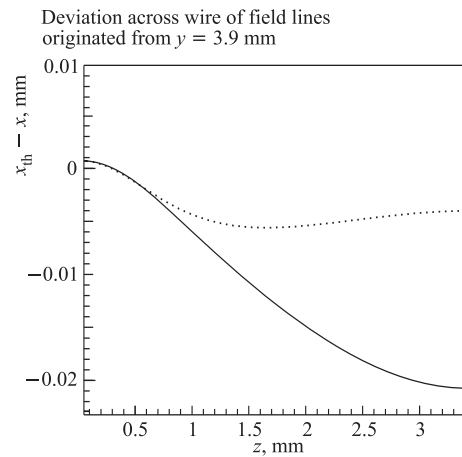


Fig. 11. Deviation of field lines from theoretical calculations

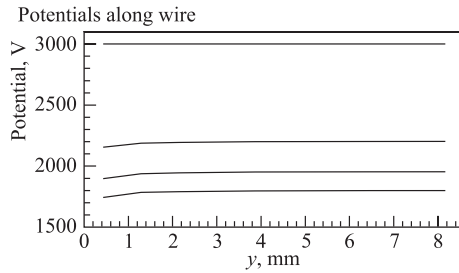


Fig. 12. Potentials along wire for different distance from wire (see text)

coordinates (theoretical and calculated) for each calculated point is presented in Fig. 11. Solid line is for the bottom field line and dashed line is for the top one. The deviation is less than $20 \mu\text{m}$.

Potential along wire is shown in Fig. 12. Abscissa zero is at the end of frames. Potentials are calculated at the surface of the wire, i.e., $15 \mu\text{m}$ from wire axis (top line), 115 , 215 and $315 \mu\text{m}$ (bottom line). There is no significant deviation in electric field magnitude due to the presence of dielectric.

5. EXPERIMENTAL RESULTS

Beside the calculations the experimental measurements of single-layer spatial resolution at the edge of the layer were made on the P3 prototype [6, 7]. The anode-cathode distance in P3 is 2.8 mm , and in the final version CSC it is 3.5 mm (see Fig. 5). Anode wire step in P3 and ME1/1 CSC is 2.5 mm . The prototype chamber P3 was placed in the muon beam of H2 channel of SPS of size $\sim 10 \times 10 \text{ cm}$. Beam axis was inclined at 10° angle to the normal of the P3 to resemble the CMS geometry. Beside that, the inclination allowed one to reject any correlations in the coordinate measurement from different layers of P3. For the gas mixture $\text{Ar}/\text{CF}_4/\text{CO}_2$ 30/20/50 and high voltage 2.9 kV the single-layer spatial resolution was investigated using the rest 5 layers as the track monitor. The results are shown in Fig. 13. One can

see that resolution at the 2nd strip is essentially the same as at the 4th strip. So, we conclude that influence of the insulating supporting frame at the edge of the layer is negligible.

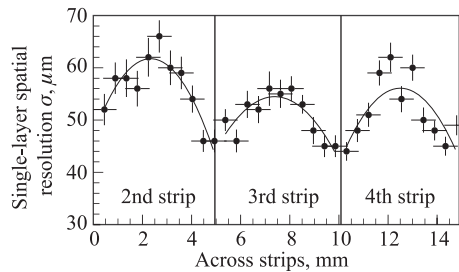


Fig. 13. Single-layer spatial resolution at the edge of the CSC

CONCLUSION

In this work the general approach to calculate electric field in the system of conductors and dielectrics is described. This approach is based on the Boundary Elements Method.

Field lines originated at $y = 3.9 \text{ mm}$ (see Fig. 8) and propagated across wire are shown in Fig. 10. Dots represent the infinite approximation same as in Fig. 7. As the wires are inclined to the insulator frames the right side of

the picture is closer to the frames than the left one. The top lines slightly deviate to the right (closer to the top frame). It is consistent with Fig. 8. For the 5th top line from the right and for the 5th bottom line from the right the deviations from the infinite approximation have been calculated. Difference between x -

Using this approach electric field at the edge of the ME1/1 CSC layer is calculated. Presence of insulator frames and inclination of anode wires to them do not significantly distort the performance of CSC in this region. So, the muon tracks that pass through the edge region of CSC could be used for standalone alignment of ME1/1 station of CMS detector.

In the end, we would like to thank A. V. Zarubin and I. A. Golutvin for arising the question about the performance of CSC at the edge and the inspiration of this work, and V. V. Perelygin for useful comments and notes.

Appendix A RECTANGULAR ELEMENT

For the rectangular element shown in Fig. 14 the following formulas for the electric field at point (x, y, z) in local reference frame were derived:

$$E_x(x, y, z) = \frac{\sigma}{4\pi\epsilon_0} \left(-\ln \left[-y + h + \sqrt{x^2 + y^2 - 2yh + h^2 - 2xw + w^2 + z^2} \right] + \right. \\ \left. + \ln \left[-y - h + \sqrt{x^2 + y^2 - 2yh + h^2 - 2xw + w^2 + z^2} \right] + \right. \\ \left. + \ln \left[-y + h + \sqrt{x^2 + y^2 - 2yh + h^2 - 2xw + w^2 + z^2} \right] - \right. \\ \left. - \ln \left[-y - h + \sqrt{x^2 + y^2 - 2yh + h^2 - 2xw + w^2 + z^2} \right] \right),$$

$$E_x(x, y, z) = \frac{\sigma}{4\pi\epsilon_0} \left(-\ln \left[x + w + \sqrt{x^2 + y^2 - 2yh + h^2 - 2xw + w^2 + z^2} \right] + \right. \\ \left. + \ln \left[-x - w + \sqrt{x^2 + y^2 - 2yh + h^2 - 2xw + w^2 + z^2} \right] + \right. \\ \left. + \ln \left[-x - w + \sqrt{x^2 + y^2 - 2yh + h^2 - 2xw + w^2 + z^2} \right] - \right. \\ \left. - \ln \left[-x - w + \sqrt{x^2 + y^2 - 2yh + h^2 - 2xw + w^2 + z^2} \right] \right),$$

$$E_x(x, y, z) = \frac{\sigma}{4\pi\epsilon_0} \left(\arctan \left[\frac{(y-h)(x-w)}{z\sqrt{(y-h)^2 + (x-w)^2 + z^2}} \right] - \right. \\ \left. - \arctan \left[\frac{(y+h)(x-w)}{z\sqrt{(y+h)^2 + (x-w)^2 + z^2}} \right] - \right.$$

$$\left. - \arctan \left[\frac{(y-h)(x+w)}{z\sqrt{(y-h)^2 + (x+w)^2 + z^2}} \right] + \arctan \left[\frac{(y+h)(x+w)}{z\sqrt{(y+h)^2 + (x+w)^2 + z^2}} \right] \right),$$

$$\begin{aligned} \phi(x, y, z) = \frac{\sigma}{4\pi\epsilon_0} & \left(-z \arctan \left[\frac{(y-h)(x-w)}{z\sqrt{x^2+y^2-2yh+h^2-2xw+w^2+z^2}} \right] + \right. \\ & + z \arctan \left[\frac{(y+h)(x-w)}{z\sqrt{x^2+y^2-2yh+h^2-2xw+w^2+z^2}} \right] + \\ & (x-w) \ln \left[y-h + \sqrt{x^2+y^2-2yh+h^2-2xw+w^2+z^2} \right] + \\ & + (y-h) \ln \left[x-w + \sqrt{x^2+y^2-2yh+h^2-2xw+w^2+z^2} \right] - \\ & (x-w) \ln \left[y+h + \sqrt{x^2+y^2-2yh+h^2-2xw+w^2+z^2} \right] + \\ & + (y+h) \ln \left[x-w + \sqrt{x^2+y^2-2yh+h^2-2xw+w^2+z^2} \right] - \\ & (x+w) \ln \left[y-h + \sqrt{x^2+y^2-2yh+h^2-2xw+w^2+z^2} \right] + \\ & + (y-h) \ln \left[x+w + \sqrt{x^2+y^2-2yh+h^2-2xw+w^2+z^2} \right] - \\ & (x+w) \ln \left[y+h + \sqrt{x^2+y^2-2yh+h^2-2xw+w^2+z^2} \right] + \\ & \left. + (y+h) \ln \left[x+w + \sqrt{x^2+y^2-2yh+h^2-2xw+w^2+z^2} \right] \right). \end{aligned}$$

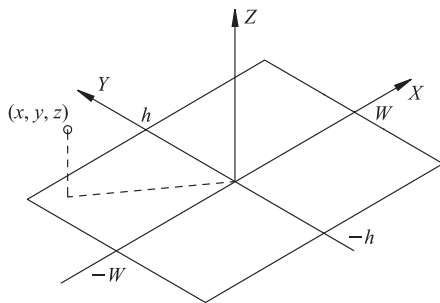


Fig. 14. Rectangular element

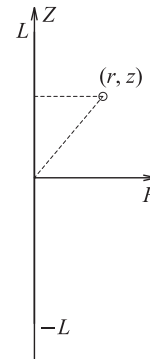


Fig. 15. Linear element

Appendix B LINEAR ELEMENT

For the linear element shown in Fig. 15 the following formulas for the electric field were derived:

$$\begin{aligned} E_r(r, z) = & \\ = \frac{\sigma}{4\pi\epsilon_0} & \frac{z \left(\sqrt{r^2 + (l-z)^2} - \sqrt{r^2 + (l+z)^2} \right) + l \left(\sqrt{r^2 + (l-z)^2} + \sqrt{r^2 + (l+z)^2} \right)}{r\sqrt{l^4 + 2l^2(r-z)(r+z) + (r^2+z^2)^2}}, \end{aligned}$$

$$E_r(r, z) = \frac{\sigma}{4\pi\epsilon_0} \frac{-\sqrt{r^2 + (l-z)^2} + \sqrt{r^2 + (l+z)^2}}{\sqrt{l^4 + 2l^2(r-z)(r+z) + (r^2 + z^2)^2}},$$

$$\phi(r, z) = \frac{\sigma}{4\pi\epsilon_0} \ln \left[l + \sqrt{r^2 + (l-z)^2} - z \right] - \ln \left[-l - z + \sqrt{r^2 + (l+z)^2} \right].$$

REFERENCES

1. *Erchov Yu. V. et al.* // Part. Nucl., Lett. 2006. V. 3, No. 3(132). P. 73–80 (in Russian).
2. *Karzhavine V. Yu. et al.* JINR Commun. P10-99-118. Dubna, 1999.
3. *Shafranov M. D., Topuria T. P.* JINR Commun. P11-99-237. Dubna, 1999.
4. «Mathematica» Code. <http://www.wolfram.com/>
5. *Petrus A. Yu., Zalikhanov B. Zh.* // Nucl. Instr. Meth. A. 2002. V. 485. P. 399–410.
6. *Erchov Yu. V. et al.* JINR Commun. E13-99-296. Dubna, 1999.
7. *Golutvin I. A. et al.* // Part. Nucl., Lett. 2001. No. 4[107]. P. 45–53.

Received on October 18, 2006.